

Modified Stranski–Krastanov growth in Ge/Si heterostructures via nanostenciled pulsed laser deposition

This article has been downloaded from IOPscience. Please scroll down to see the full text article.

2012 Nanotechnology 23 065603

(<http://iopscience.iop.org/0957-4484/23/6/065603>)

View [the table of contents for this issue](#), or go to the [journal homepage](#) for more

Download details:

IP Address: 96.22.43.228

The article was downloaded on 18/01/2012 at 12:44

Please note that [terms and conditions apply](#).

Modified Stranski–Krastanov growth in Ge/Si heterostructures via nanostenciled pulsed laser deposition

J M MacLeod¹, C V Cojocaru^{1,5}, F Ratto², C Harnagea¹, A Bernardi³, M I Alonso³ and F Rosei^{1,4}

¹ INRS, Énergie, Matériaux et Télécommunications, Université du Québec, 1650 Boulevard Lionel-Boulet, Varennes, QC, J3X 1S2, Canada

² IFAC-CNR Institute of Applied Physics, via Madonna del Piano 10, I-50019 Sesto Fiorentino, Italy

³ Institut de Ciència de Materials de Barcelona, ICMAB-CSIC, Esfera UAB, E-08193 Bellaterra, Spain

⁴ Centre for Self-Assembled Chemical Structures, McGill University, 801 Sherbrooke st. West Montreal, Quebec, H3A 2K6, Canada

E-mail: rosei@emt.inrs.ca

Received 23 September 2011, in final form 8 December 2011

Published 17 January 2012

Online at stacks.iop.org/Nano/23/065603

Abstract

The combination of nanostenciling with pulsed laser deposition (PLD) provides a flexible, fast approach for patterning the growth of Ge on Si. Within each stencilled site, the morphological evolution of the Ge structures with deposition follows a modified Stranski–Krastanov (SK) growth mode. By systematically varying the PLD parameters (laser repetition rate and number of pulses) on two different substrate orientations (111 and 100), we have observed corresponding changes in growth morphology, strain and elemental composition using scanning electron microscopy, atomic force microscopy and μ -Raman spectroscopy. The growth behaviour is well predicted within a classical SK scheme, although the Si(100) growth exhibits significant relaxation and ripening with increasing coverage. Other novel aspects of the growth include the increased thickness of the wetting layer and the kinetic control of Si/Ge intermixing via the PLD repetition rate.

 Online supplementary data available from stacks.iop.org/Nano/23/065603/mmedia

(Some figures may appear in colour only in the online journal)

1. Introduction

Despite advances in organic electronics and other novel approaches, group IV semiconductors continue to constitute the foundation of modern microelectronics. The controlled positioning of nanoscale semiconductor structures is of paramount importance to their continued use, leading to extensive studies of the self-directed formation of dot-like structures via the Stranski–Krastanov (SK) growth mode [1–4]. The possibility for novel optoelectronic devices arises with the miniaturization of device components down to the nanometre length scale, including quantum dots for

single-electron transistors, light-emitting diodes, quantum cellular automata, etc. In this context, the SK self-assembly of Ge/Si dots in epitaxially grown germanium overlayers on silicon has attracted interest due to its bottom-up parallel profile. Various features of the morphological evolution of this system have been explored in detail, including studies of the influence of kinetics versus thermodynamics [5–8] and the influence of intermixing (alloying) on growth phenomena [9–13]. Ordering and strict spatial registration of structures is essential for electronic applications, but in most cases SK islands exhibit poor lateral ordering since island nucleation is statistical in nature [14].

The growth of high-quality crystalline arrays of semiconductor nanostructures, homogeneously shaped and sized, and precisely registered on the substrate of choice, is

⁵ Present address: NRC Industrial Materials Institute, 75 de Mortagne Boulevard, Boucherville, QC, J4B 6Y4, Canada.

an intricate problem that has not been satisfactorily addressed via self-assembly alone, although efforts have capitalized on the influence of strain fields on the island nucleation or the kinetics of the growth process [15–25]. To some extent, order can be imposed on the SK growth process through the use of patterned substrates. Vicinal surfaces [26–28] and cleaved samples (cleaved edge overgrowth) [29] have been used to control nucleation. Extensive work has also been done using top-down techniques to pre-pattern surfaces for SK growth. Templates for growth have included mesas [19, 20] and holes [30, 31]. This hybrid combination of top-down pre-patterning and bottom-up SK growth provides an efficient methodology for the controlled positioning of semiconductor nanostructures. Among its drawbacks, however, is the invasiveness and increased processing time associated with the pre-patterning step, which rapidly rise with the desired precision and may reduce the potential for scale-up, such as in the case of electron or ion beam lithography [14].

In this paper we describe an alternative hybrid top-down/bottom-up approach for controlling deposition via nanostenciling, a method which selectively deposits Ge directly onto sites of predefined geometry and spacing without the need for pre-patterning the surface. Pulsed laser deposition (PLD) of Ge onto both Si(001) and (111) substrates results in the confinement of 3D island growth within predefined locations on the surface [32]. Herein, we describe a systematic study of the nanostenciled Ge/Si system. We find that the PLD-deposited Ge structures are confined exclusively to the stencil region and that the Ge nanostructures exhibit very little silicon intermixing.

2. Experimental details

A schematic of the experimental geometry is shown in figure 1. PLD was performed in vacuum ($\approx 10^{-5}$ mbar), using a GSI Lumonics KrF excimer laser unit ($\lambda = 248$ nm, $\tau = 15.4$ ns pulse FWHM) and a rotating solid Ge target (99.9% purity). Ge was deposited through the stencil onto either Si(100) (n-type, Sb-doped, resistivity of $0.015 \Omega \text{ cm}$) or Si(111) (n-type, As-doped, $0.001\text{--}0.005 \Omega \text{ cm}$). Prior to deposition, substrates were degreased and cleaned in ultrasonic solvent baths. To passivate the (100) surface, the native oxide layer was chemically removed in an aqueous HF (5%) solution, after which the samples were rinsed in deionized water and rapidly mounted in the chamber. On the Si(111) samples, a modified Shiraki cleaning method ($\text{H}_2\text{SO}_4:\text{H}_2\text{O}_2 = 4:1$ by volume) was applied prior to oxide stripping in a 5% HF solution.

Ge deposition was performed with a laser fluence of 4 J cm^{-2} and a repetition rate of either 1 or 10 Hz. The size of the laser spot on the Ge target had an average lateral dimension of 2 mm. The substrate temperature was set at 600°C , as measured with a K-type thermocouple on the heating block supporting the stencil–substrate assembly. The amount of material deposited by PLD can be easily controlled by varying the number of laser pulses for a certain target–substrate distance. The nominal deposition rate for all samples was $\approx 0.28 \text{ \AA/pulse}$, based on atomic

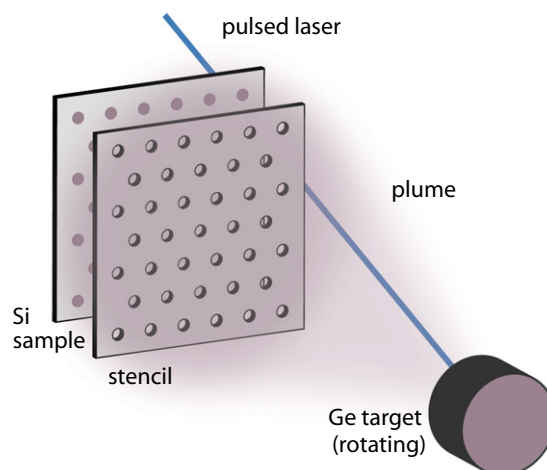


Figure 1. Simplified sketch of the sample geometry, showing the Ge target, the stencil and the Si sample.

force microscopy (AFM) measurement of the wetting layer thickness for samples near the critical thickness for 3D island growth (see supporting information, available at stacks.iop.org/Nano/23/065603/mmedia).

The stencil⁶ comprised a hexagonal pattern of circular apertures 350 nm in diameter with a pitch of 700 nm. The hexagonal pattern is contained in trenches $2 \text{ mm} \times 100 \mu\text{m}$ with an aspect ratio of approximately 4:1 (depth/width), housed in a silicon support frame. This geometry results in a thickness gradient on the structures patterned within the $100 \mu\text{m}$ wide stripe, i.e. lower-coverage structures were formed towards each edge of the patterned stripe area due to shadowing effects [33]. All data presented in this paper reflect the growth characteristics at the centre of the patterned stripe, where these shadowing effects are negligible.

The actual size of the sites patterned onto the silicon surface is dictated by the geometry of the experiment, and depends strongly on the spacing between the stencil and the sample [34]. The gap between the stencil and sample should be as small as possible, but this spacing can vary due to substrate or stencil irregularities, particulates or distortion of the stencil. In these experiments, the sample and stencil were both carefully cleaned prior to use, the stencil was held as firmly as possible against the sample and the resulting separation was inferred from the size of the stencilled features. The spacing between the substrate and the sample was not directly measured.

The same stencil was used in consecutive depositions for various numbers of ablation pulses. With repeated use, the accumulation of Ge on the stencil caused a reduction in aperture size. After ten successive depositions, corresponding to a total deposited thickness of about 300 nm, the lateral size of the deposited sites was reduced by $\approx 10\%$. The deposited Ge could be removed by dipping the stencil in warm hydrogen peroxide (H_2O_2) and subsequently rinsing in water. In trials using a similar stencil with smaller openings, we were able to produce a pattern of 96 nm germanium circles on the silicon

⁶ Stencils fabricated at Aquamarijn Filtration (The Netherlands).

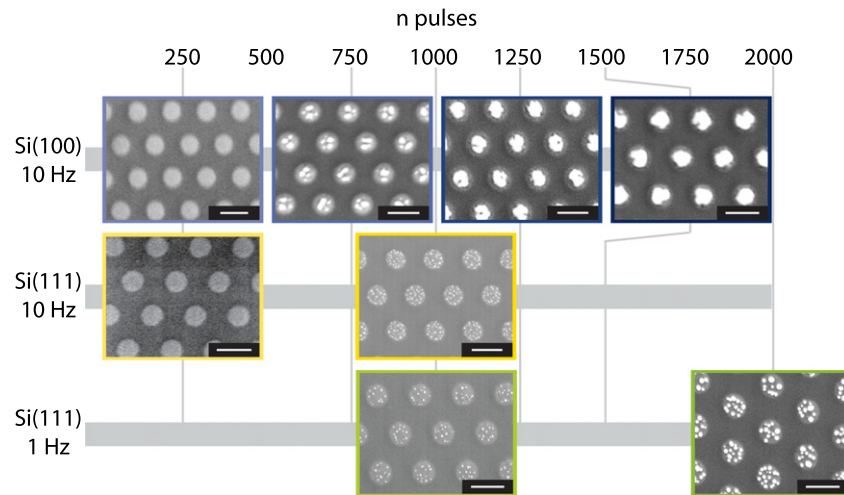


Figure 2. SEM images of patterned Ge structures formed at 600 °C via PLD through a nanostencil. Samples were fabricated on Si(100) and (111) with different numbers of PLD pulses, n , and a laser repetition rate of 10 Hz, and on Si(111) at a laser repetition rate of 1 Hz. A 500 nm scale bar is indicated in white in the lower right corner of each image.

surface using stencil openings of 85 nm diameter. However, these small openings were extremely prone to clogging, making the type of variable-coverage study described here untenable [33].

Structural characterization of the patterned Ge islands was performed via contact-mode AFM, using a Veeco Nanoprobe equipped with a general purpose cantilever (Si_3N_4 , tip apex radius 20 nm) and scanning electron microscopy (SEM), using a JEOL JSM-6300F. SEM and AFM images were calibrated via the 700 nm pitch of the stencilled sites. Further information was obtained from micro-Raman spectroscopy, a surface-sensitive technique particularly suitable to extract information about elemental composition and strain inside group IV semiconductor nanostructures [35, 36]. The Raman measurements were carried out at room temperature by probing the patterned area with the 514.5 nm line of an Ar^+ ion laser focused with a spot size of about 1 μm , i.e. each spectrum is collected from a few stencil sites.

3. Results

To systematically investigate the growth processes of stencilled Ge on Si, a number of samples were prepared under different conditions. Figure 2 shows SEM images obtained from each of the samples.

At low Ge coverage, smooth 2D mounds are formed on both Si(100) and (111). The SEM images in figure 2 illustrate this growth at 250 laser ablation pulses (equivalent deposited thickness ≈ 7 nm). AFM measurements indicate typical thicknesses for the smooth wetting layer of 6–7 nm on the (100) surface and 3–5 nm on the (111) surface. The substrate region between the stencil sites remains flat and uniform.

Beyond the critical (wetting layer) thickness, growth proceeds through the formation of three-dimensional islands. The morphology of these islands is markedly different

between the Si(100) and (111) surfaces: whereas each stencil site on Si(100) hosts a small number of large islands that gradually coalesce with increasing Ge coverage, the islands on (111) are smaller and remain discrete to at least 2000 laser pulses, corresponding to a nominal thickness of 56 nm. AFM measurements (not shown) do not reveal well-defined faceting on the 3D islands on either substrate but indicate that the maximum height of the islands increases with coverage. The maximum island height, measured from the wetting layer, increases from 32 ± 4 nm at 750 pulses to 53 ± 4 nm at 1250 pulses on Si(100), and from 20 ± 4 nm at 1000 pulses to 42 ± 5 nm at 2000 pulses on Si(111) (1 Hz). Variation in the laser repetition rate was also found to affect the island growth. For the structures grown on Si(111), 1000 pulses at 1 Hz (figure 2) produced fewer larger dots than in the counterpart sample prepared at 10 Hz.

Statistical analysis of the SEM images confirms these qualitative trends, as shown in figure 3. On Si(100) the distribution in the number of dots per site shows an average of ≈ 3 , with a standard deviation of ≈ 1 , for 750 pulses. The mean number of islands converges towards unity with increasing coverage of Ge. Conversely, the statistics for the 1 Hz samples on (111) show less sensitivity to coverage. The distributions have means of ≈ 11 , for both 1000 and 2000 pulses, with the standard deviation slightly increasing from 2.1 to 2.5, respectively. The distribution for the sample grown at 10 Hz has a higher mean number of islands, ≈ 24 , with a relatively small standard deviation of 2.2.

The corresponding major axis lengths for the 3D islands are shown in figure 4. The samples prepared on Si(100) have much larger islands than the samples prepared on Si(111). The (100) islands sizes are broadly distributed after 750 pulses, with an average size of 115 nm, and a standard deviation of 49 nm. Increasing the Ge coverage to 1250 pulses increases the average island size to 315 nm, with the distribution narrowing to a standard deviation of 40 nm. Finally, at 1500 pulses, the island size converges towards 274 nm, with a

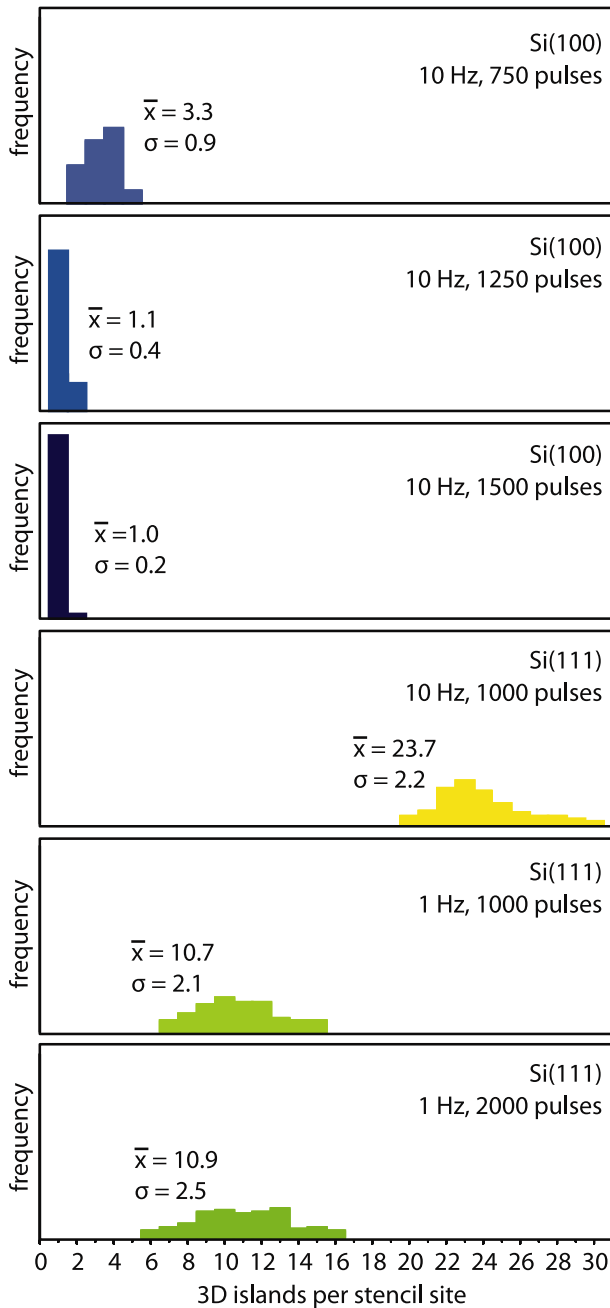


Figure 3. Number of 3D islands per stencil site for samples similar to those shown in figure 2. The mean and standard deviation for each of the normalized distributions is shown in the figure.

standard deviation of 25 nm. The increase in lateral size with coverage is less pronounced on the Si(111) substrate. In going from 1000 to 2000 pulses, the mean size increases from 28 nm to 53 nm, accompanied by a broadening of the size distribution.

The average diameters for the stencilled sites are also shown in figure 4. The site size varied from ≈ 410 nm for the samples grown on Si(111) at 1 Hz, as well as the 1500 pulse Si(100) sample, to 490 nm for the 1250 pulse, Si(100) sample.

The μ -Raman spectra are shown in figure 5. The spectra are consistent with those expected for Si/Ge hybrid structures [37], and we assign the dominant phonon peaks

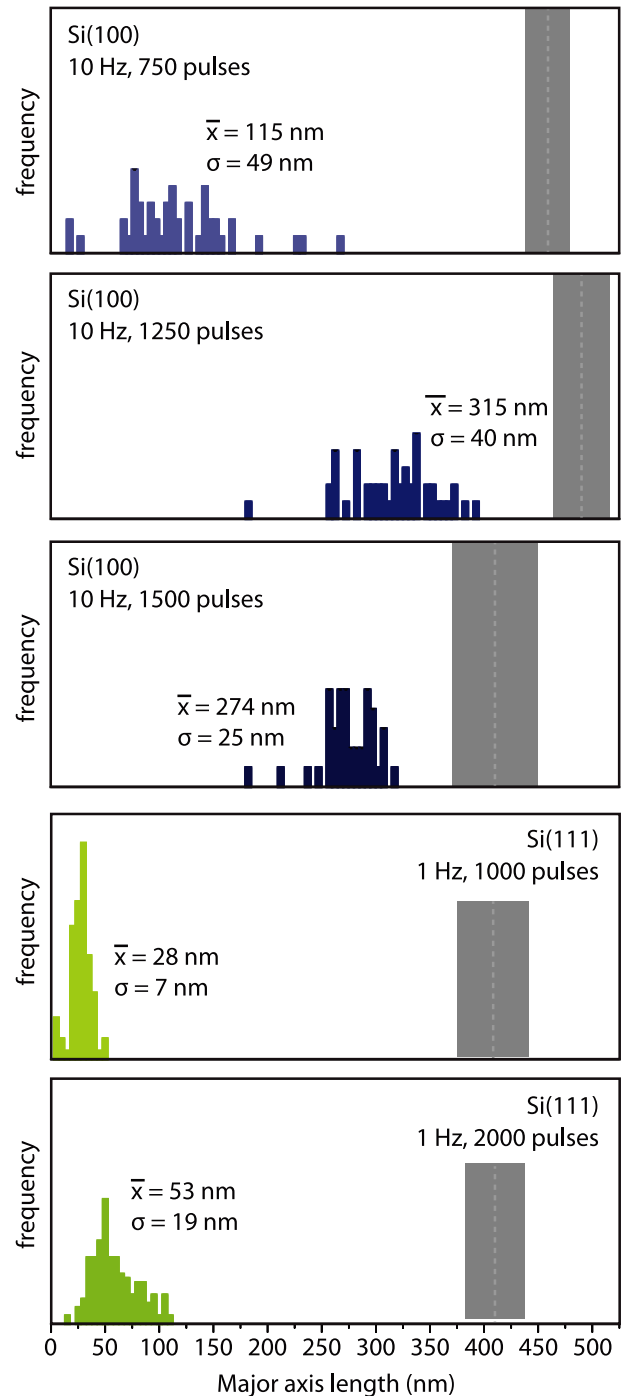


Figure 4. Major axis length distributions of 3D islands for samples similar to those shown in figure 2. The mean and standard deviation for each of the normalized distributions is shown in the figure. The dashed lines indicate the average diameter of the stencilled sites for each sample.

accordingly: Ge–Ge at ≈ 300 cm^{-1} , Si–Si at 520 cm^{-1} and Ge–Si at ≈ 400 cm^{-1} . The spectra from the samples grown on Si(100) do not contain a Si–Ge peak, indicating no detectable intermixing. On these samples, the Ge–Ge peak shifts down in frequency as the number of pulses increases, consistent with a progressive relaxation of strain with increasing coverage. Notable features of the spectra obtained from Si(111) include the presence of a Ge–Si peak for the samples prepared at 1 Hz,

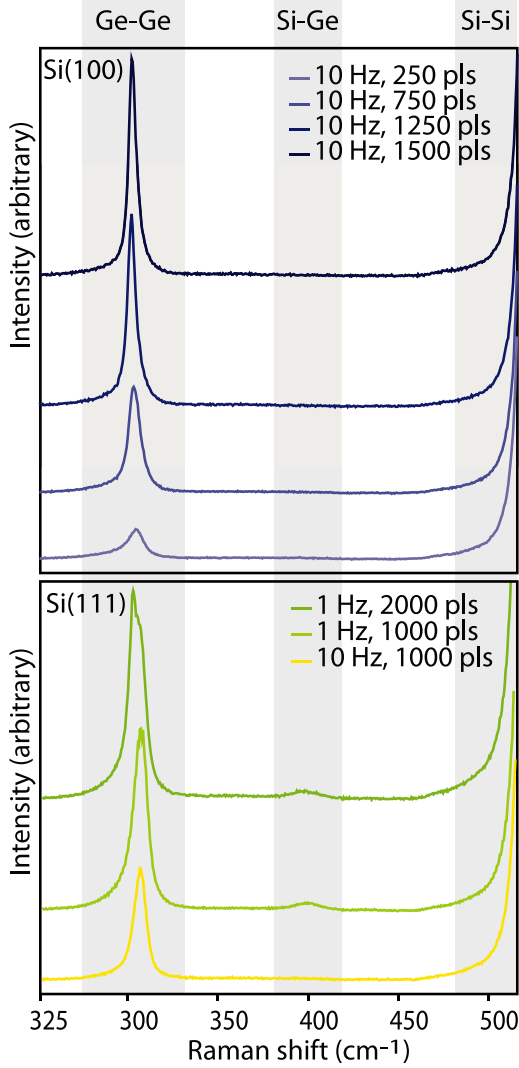


Figure 5. μ -Raman spectra for Ge patterned onto Si(100) (top) and Si(111) (bottom). The approximate locations of the Ge–Ge, Ge–Si and Si–Si peaks are identified with grey shading. The traces have been offset from one another for clarity.

indicating Si–Ge intermixing, and the separation of the Ge–Ge peak into two components, which is particularly marked in the 2000-pulse sample. As in the case of the Si(100) samples, no intermixing is detected in the sample prepared at 10 Hz.

The phonon peaks in figure 5 were fitted with Lorentzian functions, and the spectral positions obtained for the Ge–Ge and Si–Ge peaks (in cm^{-1}) were used to calculate the composition (x) of the $\text{Si}_{1-x}\text{Ge}_x$ alloy and the in-plane strain (ϵ_{\parallel}) by applying the empirical relations from [36]:

$$\omega_{\text{Ge-Ge}} = 284 + 5x + 12x^2 + b_{\text{Ge-Ge}}\epsilon_{\parallel} \quad (1)$$

$$\omega_{\text{Si-Ge}} = 400 + 29x - 95x^2 + 213x^3 - 170x^4 + b_{\text{Si-Ge}}\epsilon_{\parallel}. \quad (2)$$

For samples grown on Si(100) we used the values of the phonon strain-shift coefficients $b_{\text{Ge-Ge}}(100) \approx -460 \text{ cm}^{-1}$ and $b_{\text{Si-Ge}}(100) \approx -555 \text{ cm}^{-1}$, determined by Reparaz *et al* [38]. For samples grown on Si(111) the biaxial strain splits

Table 1. In-plane strain (ϵ_{\parallel}) and composition (x) of the $\text{Si}_{1-x}\text{Ge}_x$ alloy extracted from μ -Raman data.

Sample	$\omega_{\text{Ge-Ge}}$ (cm^{-1})	$\omega_{\text{Si-Ge}}$ (cm^{-1})	ϵ_{\parallel}	x
Si(100)				
10 Hz, 250 pulses	302.7	—	$-0.4\% \pm 0.2\%$	1
10 Hz, 750 pulses	302.4	—	$-0.3\% \pm 0.2\%$	1
10 Hz, 1250 pulses	301.0	—	$0\% \pm 0.2\%$	1
10 Hz, 1500 pulses	301.4	—	$-0.1\% \pm 0.2\%$	1
Si(111)				
1 Hz, 1000 pulses	304.7	396.4	$-1.2\% \pm 0.2\%$	0.93 ± 0.2
1 Hz, 2000 pulses	300.9	—	0	1
	305.7	395.5	$-1.4\% \pm 0.2\%$	0.94 ± 0.2
10 Hz, 1000 pulses	304.4	—	$-0.7\% \pm 0.2$	1

the triply degenerated LO–TO optical phonon branches into two components: a singlet LO and a doublet TO branch. We calculated the phonon strain-shift coefficients for these modes as explained in [39] using the phonon deformation potentials p and q from [38]. The two different notations are related by $\tilde{K}_{11} = p/\omega_0^2$, $\tilde{K}_{12} = q/\omega_0^2$. The component $\tilde{K}_{44} = r/\omega_0^2$ was taken to be that of Ge for the Ge–Ge mode and the average of the Si and Ge values for the Si–Ge mode [38]. The resulting strain-shift coefficients are $b_{\text{Ge-Ge}}(111, d) \approx -668 \text{ cm}^{-1}$, $b_{\text{Ge-Ge}}(111, s) \approx -152 \text{ cm}^{-1}$, $b_{\text{Si-Ge}}(111, d) \approx -835 \text{ cm}^{-1}$ and $b_{\text{Si-Ge}}(111, s) \approx -307 \text{ cm}^{-1}$, where d and s stand for doublet and singlet, respectively. Although one of the samples on Si(111) showed a double peak, cf figure 5, this splitting is not attributed to these two components. In fact, in the experiments we could not resolve the singlet because the observed peak positions were almost insensitive to polarization. Therefore, the Raman modes that we observe on the Si(111) samples must correspond to the more intense doublet TO modes only [39]. Using the strain-shift coefficients given above we obtained the composition and strain values as tabulated in table 1.

4. Discussion

4.1. Stencilling as a methodology

The circular profile of the deposited regions of Ge directly reproduces the shape of the apertures in the stencil. This fidelity may be linked to a combination of effects: (i) a strong confinement of the PLD-generated Ge flux, (ii) limited diffusion across the substrate (see below) and (iii) enhanced corner diffusion, observed to take place when highly energetic species arrive at the substrate [40], which promotes circular structures. The confinement of the Ge flux is further indicated by the lack of observable structures on the substrate between the stencil sites. This is seen to occur despite the fact that typical Ge diffusion lengths [41] on clean Si at 600°C should range from $\approx 2 \times 10^2 \text{ nm}$ (Si(111), 250 pulses) to as much as $\approx 2 \times 10^4 \text{ nm}$ (Si(100), 1750 pulses). The lack of island growth

between the stencil sites may be due to inhibition of either diffusion or nucleation in these regions, which could occur due to the presence of an oxide layer, as has been observed, for example, in nanostructured oxide patterns [42]. We note that under ultrahigh vacuum conditions, where oxide formation is negligible, Sn and Ag are observed to diffuse hundreds of nanometres from similar stencil sites on Si(100) [34]. In our experiments, the presence of O₂ in the relatively high chamber background pressure leads to the dynamic development of the oxide at high temperature, which appears to passivate the regions of the Si substrate between the aperture sites against Ge growth. This effect is suppressed within the stencil sites by the direct flux of energetic Ge impinging on the surface.

For all samples, the size of the patterned regions on the substrate was larger than the 350 nm opening in the stencil. This spreading is a geometrical consequence of the experimental geometry, and for our fixed source–sample spacing, depends on two variables: the size of the source, i.e. the size of the laser spot on the target and the spacing between the stencil and the sample (see supporting information, available at stacks.iop.org/Nano/23/065603/mmedia). Taking the average laser spot size of 2 mm, the corresponding sample–substrate spacings were estimated to be between 1.8 and 4.2 μm , although it is not obvious whether the variation in the size of the patterned sites is solely due to differences in the stencil positioning, or whether fluctuation in the laser spot size also contributed.

4.2. Growth mechanisms

Wetting layer. The stencilled growth of Ge on Si can be described as a modified Stranski–Krastanov process. In conventional SK growth, typically observed critical values are 2–3 atomic bilayers (0.63–0.95 nm) for Ge on Si(111) [43] or 3–5 monolayers (0.4–0.68 nm) for Ge on Si(001) [44]. Our observed values are about five times larger for the (111) surface and about ten times larger for the (100) surface. These anomalously high critical thickness for the onset of 3D nucleation can be explained by invoking the small size of the deposited areas. The discrete sites may benefit from mechanisms for lateral strain relief at their periphery, thus delaying the strain-induced 3D nucleation of islands [45]. The fact that we see a thicker wetting layer on (100), as opposed to (111), may indicate that dislocation nucleation is more facile on the (100)-oriented stencil sites.

Island nucleation and growth. In traditional SK growth of Ge on Si, the nucleation of the 3D islands occurs nearly simultaneously across the substrate [46]. Nucleation is a statistical process which requires a critical density of mobile atoms. In turn the density of mobile atoms results from the competition of deposition and capture from the growing islands. Therefore nucleation ends when the separation between the islands becomes a fraction of the diffusion length of the mobile atoms, with the exact value depending on factors such as the deposition rate, diffusivity and critical size of stable nuclei [14]. After nucleation, the islands continue to grow at constant density at least until ripening begins.

Consistent with this picture, the histograms in figure 3 show that, at 1 Hz, the density of 3D islands per site has nearly identical values for 1000 and 2000 pulses. Evaluation of the size distribution for the same samples (figure 4) shows a fairly narrow distribution in the case of the sample prepared for 1000 pulses with a mean value of 28 nm, whereas a mean value of 53 nm (major length) and a broader distribution is found for the islands grown at 2000 pulses. This broader size distribution at 2000 pulses is not an immediate consequence of growth kinetics, and may point to the onset of Ostwald ripening. The increase in average size with deposition is clearly associated with SK growth at constant island density. However, the increase of island width occurs significantly faster than expected for expansion occurring exclusively from the deposited material (i.e. the size does not scale as expected with the number of pulses beyond the wetting layer), suggesting the possibility of additional material sources for island growth, such as from the erosion of the wetting layer [47, 48].

The higher density of islands for the same substrate at a PLD repetition rate of 10 Hz is clearly associated with a higher incidence of nucleation, which results from the higher supply of mobile atoms at constant diffusivity feeding their density. The increased deposition rate also has a direct impact on the nucleation density. As shown in figure 3, for samples prepared on Si(111) at 1000 pulses, a laser repetition rate of 1 Hz produces roughly half the density of dots produced at a rate of 10 Hz. This is consistent with the power law increase in nuclei density with deposition rate, which occurs as a general consequence of SK kinetics [49–52].

The nucleation behaviour on the Si(100) surface is markedly different, as shown by the small number of islands on the 750-pulse sample. This decreased nucleation density may be due to an enhanced diffusion and possibly a larger critical size for the stable nuclei under the specific conditions imposed by nanostenciling. Contrary to the Si(111) samples, which do not show a marked change in island density with coverage, islands on the (100) samples are observed to ripen and coalesce with increasing coverage, finally converging to a single island per stencil site at 1500 pulses. This is also consistent with increased diffusivity, and may also be influenced by the nearly complete strain relaxation (see below for further discussion).

Island crystallinity, composition and strain. The Raman data for these samples provide more insight into the mechanisms underlying the observed morphologies. The spectral shape and position of the Ge–Ge phonon mode (figure 5) indicates that all patterned structures are crystalline. The blueshifting of the peak away from the bulk value at around 301 cm^{-1} indicates the presence of compressive strain, a hallmark of Ge/Si epitaxial growth. Another important feature of the recorded spectra is the Si–Ge peak, observed for the samples prepared at 1 Hz, which implies Si–Ge intermixing. Table 1 tabulates the calculated intermixing and strain based on the locations of these peaks. The 1000-pulse sample has $x = 0.93 \pm 0.2$ and is compressively strained by $-1.2 \pm 0.2\%$. The 2000-pulse peak contains two components. The

low-frequency component indicates slightly less intermixing ($x = 0.94 \pm 0.2$) than the 1000-pulse sample, as well as a slight increase in strain ($-1.4 \pm 0.2\%$). However, most of the intensity in the Ge–Ge peak for the 2000-pulse sample is contributed by an unstrained, pure Ge component⁷. The emergence of this component may be due to the rearrangement of the strained islands indicated at 1000 pulses, e.g. due to the nucleation of misfit dislocations above a critical island size and/or a feature of the additional material deposited onto the islands, which may or may not maintain the epitaxial relationship to the substrate.

The unusually large thickness of the wetting layer in these experiments precludes some of the conventional mechanisms for the relaxation of Ge dots on Si, which rely on the sourcing of Si from the substrate [53], so the relaxation of these islands must depend heavily on the formation of dislocations. It is also interesting to note that, using traditional growth methodologies, it can be difficult to produce Ge-rich structures in Ge/Si growth, since energetics favour the intermixing of Si into Ge (but not vice versa) [54]. Hence, this growth methodology provides access to a stoichiometric regime not normally achieved.

The Si–Ge peak is absent from the Raman spectra for all the samples prepared on (111) at 10 Hz, suggesting that the Si–Ge intermixing is kinetically suppressed. This is confirmed through the lack of intermixing observed for the Si(100) samples, all of which were prepared at 10 Hz.

According to table 1, an almost complete relaxation of the misfit strain occurs for the samples grown on Si(100). This relaxation plays a critical role in the growth and ripening of the islands and enables large lateral sizes and coalescence, with the structure evolving to a single island per site on the samples grown at 1500 pulses. Interestingly the coalescence of these islands is accompanied by some anomalous behaviour, with the mean length decreasing and the misfit strain increasing slightly in going from 1250 to 1500 pulses. Together, these changes indicate ripening, which smooths asperities that may have contributed to the size and very efficient strain relief for the 1250-pulse sample. The lateral width of the wetting layer correspondingly decreases between the 1250- and 1500-pulse samples, further suggesting that these large, ripened islands are directly size-constrained according to the diameter of the patterned sites.

5. Conclusions and outlook

The stencilled PLD growth of Ge on Si provides new opportunities for controlling the growth of nanoscale group IV structures. The stencil used in this study produced a pattern of circular structures, each ≈ 15 –40% larger than the 350 nm stencil openings. Since this spreading depends on both the evaporation source size and the distance between the stencil

and the sample, it can presumably be minimized by reducing the size of the laser spot on the PLD target, while at the same time taking care to ensure good sample–stencil contact.

Within each stencil site, the growth process is largely consistent with SK growth, and begins with the formation of a thick wetting layer. The layer thickness was slightly larger for (100) samples than (111), suggesting that strain relief via dislocation formation occurs more easily on the former. The completion of the wetting layer is followed by the nucleation of three-dimensional islands. On Si(111), the island density is found to be higher for a 10 Hz PLD repetition rate than for a 1 Hz rate, and the density does not change with coverage, as expected within the SK regime. On Si(100), the initial nucleation density is much lower than on (111), and the evolution of growth with coverage is strongly dominated by coalescence and ripening. For the highest-coverage samples studied, the final structure evolved to a single island, the size of which appeared to be directly related to the size of the stencilled site. The μ -Raman measurements indicate that the structures on Si(100) are nearly fully relaxed, whereas more strain is present in all of the samples on (111).

This approach produces novel growth characteristics when compared to its conventional counterparts. The anomalously thick wetting layer may suppress Si intermixing into the 3D islands and the PLD repetition rate can further be adjusted to suppress intermixing. The oxide-covered substrate regions between the stencil sites did not exhibit any Ge accumulation, providing for excellent fidelity in the transfer of the stencil pattern. These factors could make this method attractive for the production of Si–Ge islands with a Ge-rich stoichiometry, which provides a counterpoint to other patterning methods that promote silicon intermixing [55].

Acknowledgments

The authors acknowledge financial support from the Canada Foundation for Innovation, and NSERC of Canada. FR is grateful to FQRNT and the Canada Research Chairs programme for salary support. AB acknowledges an FPI fellowship. JM was supported by an NSERC postdoctoral fellowship. This work was supported in part by the Spanish Ministry of Science and Innovation (MICINN) through grant MAT2009-09480. We thank Josh Lipton-Duffin for his assistance with the composition and strain calculations.

References

- [1] Eaglesham D J and Cerullo M 1990 Dislocation-free Stranski–Krastanov growth of Ge on Si(100) *Phys. Rev. Lett.* **64** 1943–6
- [2] Mo Y W, Savage D E, Swartzentruber B S and Lagally M G 1990 Kinetic pathway in Stranski–Krastanov growth of Ge on Si(001) *Phys. Rev. Lett.* **65** 1020–3
- [3] Leonard D, Krishnamurthy M, Reaves C M, Denbaars S P and Petroff P M 1993 Direct formation of quantum-sized dots from uniform coherent islands of InGaAs on GaAs-surfaces *Appl. Phys. Lett.* **63** 3203–5
- [4] Stangl J, Holy V and Bauer G 2004 Structural properties of self-organized semiconductor nanostructures *Rev. Mod. Phys.* **76** 725–83

⁷ This interpretation rests on the association of the observed Si–Ge peak with the higher-frequency component of the Ge–Ge peak and the assumption that the lower-frequency Ge–Ge component is not associated with any intermixing. Although the frequency of the corresponding singlet would be 300.7 cm^{-1} , both the high intensity of the observed peak and the absence of a split Si–Ge peak reinforce the given interpretation.

- [5] Williams R S, Medeiros-Ribeiro G, Kamins T I and Ohlberg D A A 1999 Chemical thermodynamics of the size and shape of strained Ge nanocrystals grown of Si(001) *Acc. Chem. Res.* **32** 425–33
- [6] Medeiros-Ribeiro G, Bratkovski A M, Kamins T I, Ohlberg D A A and Williams R S 1998 Shape transition of germanium nanocrystals on a silicon (001) surface from pyramids to domes *Science* **279** 353–5
- [7] Ross F M, Tersoff J and Tromp R M 1998 Coarsening of self-assembled Ge quantum dots on Si(001) *Phys. Rev. Lett.* **80** 984–7
- [8] Rosei F and Rosei R 2002 Atomic description of elementary surface processes: diffusion and dynamics *Surf. Sci.* **500** 395–413
- [9] Boscherini F, Capellini G, Di Gaspare L, Rosei F, Motta N and Mobilio S 2000 Ge–Si intermixing in Ge quantum dots on Si(001) and Si(111) *Appl. Phys. Lett.* **76** 682–4
- [10] Boscherini F, Capellini G, Di Gaspare L, De Seta M, Rosei F, Sgarlata A, Motta N and Mobilio S 2000 Ge–Si intermixing in Ge quantum dots on Si *Thin Solid Films* **380** 173–5
- [11] Ratto F, Rosei F, Locatelli A, Cherifi S, Fontana S, Heun S, Szkutnik P D, Sgarlata A, De Crescenzi M and Motta N 2004 Composition of Ge(Si) islands in the growth of Ge on Si(111) *Appl. Phys. Lett.* **84** 4526–8
- [12] Ratto F, Costantini G, Rastelli A, Schmidt O G, Kern K and Rosei F 2006 Alloying of self-organized semiconductor 3D islands *J. Exp. Nanosci.* **1** 279–305
- [13] MacLeod J M, Lipton-Duffin J A, Lanke U, Urquhart S G and Rosei F 2009 Shape transition in very large germanium islands on Si(111) *Appl. Phys. Lett.* **94** 103109
- [14] Ratto F and Rosei F 2010 Order and disorder in the heteroepitaxy of semiconductor nanostructures *Mater. Sci. Eng. R* **70** 243–64
- [15] Kamins T I and Williams R S 1997 Lithographic positioning of self-assembled Ge islands on Si(001) *Appl. Phys. Lett.* **71** 1201–3
- [16] Kamins T I, Ohlberg D A A, Williams R S, Zhang W and Chou S Y 1999 Positioning of self-assembled, single-crystal, germanium islands by silicon nanoimprinting *Appl. Phys. Lett.* **74** 1773–5
- [17] Vescan L 2001 SiGe nanostructures by selective epitaxy and self-assembling *Mater. Sci. Eng. A* **302** 6–13
- [18] Kim E S, Usami N and Shiraki Y 1998 Control of Ge dots in dimension and position by selective epitaxial growth and their optical properties *Appl. Phys. Lett.* **72** 1617–9
- [19] Jin G, Liu J L, Thomas S G, Luo Y H, Wang K L and Nguyen B Y 1999 Controlled arrangement of self-organized Ge islands on patterned Si(001) substrates *Appl. Phys. Lett.* **75** 2752–4
- [20] Jin G, Liu J L and Wang K L 2000 Regimented placement of self-assembled Ge dots on selectively grown Si mesas *Appl. Phys. Lett.* **76** 3591–3
- [21] Zhong Z Y, Halilovic A, Muhlberger M, Schaffler F and Bauer G 2003 Positioning of self-assembled Ge islands on stripe-patterned Si(001) substrates *J. Appl. Phys.* **93** 6258–64
- [22] Schmidt O G, Jin-Phillipp N Y, Lange C, Denker U, Eberl K, Schreiner R, Grabeldinger H and Schweizer H 2000 Long-range ordered lines of self-assembled Ge islands on a flat Si(001) surface *Appl. Phys. Lett.* **77** 4139–41
- [23] Vescan L 2002 Ge nanostructures grown by self-assembly; influence of substrate orientation *J. Phys.: Condens. Matter* **14** 8235–52
- [24] Karmous A, Cuenat A, Ronda A, Berbezier I, Atha S and Hull R 2004 Ge dot organization on Si substrates patterned by focused ion beam *Appl. Phys. Lett.* **85** 6401–3
- [25] Bernardi A, Alonso M I, Goni A R, Osso J O and Garriga M 2006 Density control on self-assembling of Ge islands using carbon-alloyed strained SiGe layers *Appl. Phys. Lett.* **89** 101921
- [26] Ogino T, Hibino H and Homma Y 1997 Step arrangement design and nanostructure self-organization on Si surfaces *Appl. Surf. Sci.* **117** 642–51
- [27] Zhu J H, Brunner K and Abstreiter G 1998 Two-dimensional ordering of self-assembled Ge islands on vicinal Si(001) surfaces with regular ripples *Appl. Phys. Lett.* **73** 620–2
- [28] Sakamoto K, Matsuhata H, Tanner M O, Wang D W and Wang K L 1998 Alignment of Ge three-dimensional islands on faceted Si(001) surfaces *Thin Solid Films* **321** 55–9
- [29] Arai J, Usami N, Ota K, Shiraki Y, Ohga A and Hattori T 1997 Precise control of island formation using overgrowth technique on cleaved edges of strained multiple quantum wells *Appl. Phys. Lett.* **70** 2981–3
- [30] Zhong Z, Schmidt O G and Bauer G 2005 Increase of island density via formation of secondary ordered islands on pit-patterned Si(001) substrates *Appl. Phys. Lett.* **87** 133111
- [31] Chen G, Lichtenberger H, Bauer G, Jantsch W and Schaeffler F 2006 Initial stage of the two-dimensional to three-dimensional transition of a strained SiGe layer on a pit-patterned Si(001) template *Phys. Rev. B* **74** 035302
- [32] Cojocaru C V, Bernardi A, Reparaz J S, Alonso M I, MacLeod J M, Harnagea C and Rosei F 2007 Site-controlled growth of Ge nanostructures on Si(100) via pulsed laser deposition nanostenciling *Appl. Phys. Lett.* **91** 113112
- [33] Cojocaru C V 2007 Controlled growth and positioning of functional materials by unconventional nanoscale patterning *PhD Thesis* Université du Québec INRS-EMT
- [34] Linklater A and Nogami J 2008 Defining nanoscale metal features on an atomically clean silicon surface with a stencil *Nanotechnology* **19** 285302
- [35] Bernardi A, Osso J O, Alonso M I, Goni A R and Garriga M 2006 Influence of Si interdiffusion on carbon-induced growth of Ge quantum dots: a strategy for tuning island density *Nanotechnology* **17** 2602–8
- [36] Alonso M I, de la Calle M, Osso J O, Garriga M and Goni A R 2005 Strain and composition profiles of self-assembled Ge/Si(001) islands *J. Appl. Phys.* **98** 033530
- [37] Jain S C and Hayes W 1991 Structure, properties and applications of $\text{Ge}_x\text{Si}_{1-x}$ strained layers and superlattices *Semicond. Sci. Technol.* **6** 547–76
- [38] Reparaz J S, Bernardi A, Goni A R, Alonso M I and Garriga M 2008 Composition dependence of the phonon strain shift coefficients of SiGe alloys revisited *Appl. Phys. Lett.* **92** 081909
- [39] Mermoux M, Crisci A, Baillet F, Destefanis V, Rouchon D, Papon A M and Hartmann J M 2010 Strain in epitaxial Si/SiGe graded buffer structures grown on Si(100), Si(110), and Si(111) optically evaluated by polarized Raman spectroscopy and imaging *J. Appl. Phys.* **107** 013512
- [40] Amar J G 1999 Mechanisms of mound coarsening in unstable epitaxial growth *Phys. Rev. B* **60** 11317–20
- [41] Dolbak A E and Olshanetsky B Z 2006 Ge diffusion on Si surfaces *Cent. Euro. J. Phys.* **4** 310–7
- [42] Robinson J T, Ratto F, Moutanabbir O, Heun S, Locatelli A, Mentès T O, Aballe L and Dubon O D 2007 Gold-catalyzed oxide nanopatterns for the directed assembly of Ge island arrays on Si *Nano Lett.* **7** 2655–9
- [43] Voigtlander B 2001 Fundamental processes in Si/Si and Ge/Si epitaxy studied by scanning tunneling microscopy during growth *Surf. Sci. Rep.* **43** 127
- [44] Brehm M *et al* 2009 Key role of the wetting layer in revealing the hidden path of Ge/Si(001) Stranski–Krastanov growth onset *Phys. Rev. B* **80** 205321
- [45] Kukta R V 2010 Mechanics of quantum-dot self-organization by epitaxial growth on small areas *J. Appl. Mech. Trans. ASME* **77** 041001

- [46] Shklyav A A, Shibata M and Ichikawa M 1998 Ge islands on Si(111) at coverages near the transition from two-dimensional to three-dimensional growth *Surf. Sci.* **416** 192–9
- [47] Joyce P B, Krzyzewski T J, Bell G R, Joyce B A and Jones T S 1998 Composition of InAs quantum dots on GaAs(001): direct evidence for (In, Ga) As alloying *Phys. Rev. B* **58** 15981–4
- [48] Patella F, Arciprete F, Fanfoni M, Sessi V, Balzarotti A and Placidi E 2005 Reflection high energy electron diffraction observation of surface mass transport at the two- to three-dimensional growth transition of InAs on GaAs(001) *Appl. Phys. Lett.* **87** 252101
- [49] Venables J A, Derrien J and Janssen A P 1980 Direct observation of the nucleation and growth modes of Ag/Si(111) *Surf. Sci.* **95** 411–30
- [50] Venables J A, Spiller G D T and Hanbucken M 1984 Nucleation and growth of thin films *Rep. Prog. Phys.* **47** 399
- [51] Sullivan J S, Evans H, Savage D E, Wilson M R and Lagally M G 1999 Mechanisms determining three-dimensional SiGe island density on Si(001) *J. Electron. Mater.* **28** 426–31
- [52] Capellini G, De Seta M and Evangelisti F 2003 Ge/Si(100) islands: Growth dynamics versus growth rate *J. Appl. Phys.* **93** 291–5
- [53] Smith D J, Chandrasekhar D, Chaparro S A, Crozier P A, Drucker J, Floyd M, McCartney M R and Zhang Y 2003 Microstructural evolution of Ge/Si(100) nanoscale islands *J. Cryst. Growth* **259** 232–44
- [54] Schorer R, Friess E, Eberl K and Abstreiter G 1991 Structural stability of short-period Si/Ge superlattices studied with Raman-spectroscopy *Phys. Rev. B* **44** 1772–81
- [55] Chen G, Vastola G, Zhang J J, Sanduijav B, Springholz G, Jantsch W and Schaeffler F 2011 Enhanced intermixing in Ge nanoprisms on groove-patterned Si(1110) substrates *Appl. Phys. Lett.* **98** 023104